Nanoelectronics and Its New Materials – A NEW ERA OF NANOSCIENCE

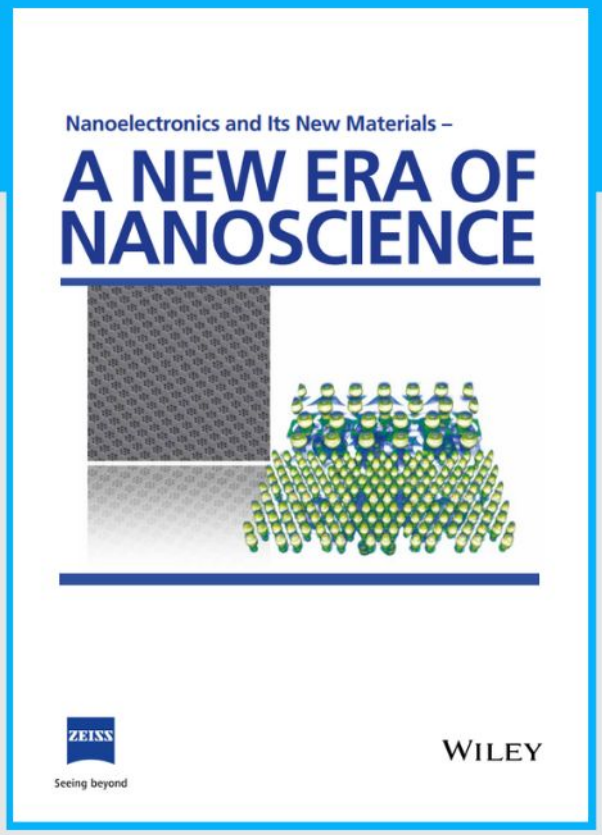

Discover the recent advances in electronics research and fundamental nanoscience.

Nanotechnology has become the driving force behind breakthroughs in engineering, materials science, physics, chemistry, and biological sciences. In this compendium, we delve into a wide range of novel applications that highlight recent advances in electronics research and fundamental nanoscience. From surface analysis and defect detection to tailored optical functionality and transparent nanowire electrodes, this eBook covers key topics that will revolutionize the future of electronics.

To get your hands on this valuable resource and unleash the power of nanotechnology, simply download the eBook now. Stay ahead of the curve and embrace the future of electronics with nanoscience as your guide.

ZEISS

Seeing beyond

WILEY

RESEARCH ARTICLE

NANO · MICRO small
www.small-journal.com

Bone-Targeted Biomimetic Nanogels Re-Establish Osteoblast/Osteoclast Balance to Treat Postmenopausal Osteoporosis

Yongzhi Cui, Bin Lv, Zhongying Li, Chunming Ma, Zhengwei Gui, Yongtao Geng, Guohui Liu, Linchao Sang, Chen Xu, Qi Min, Li Kong, Zhiping Zhang, Yang Liu, Xiangbei Qi,* and Dehao Fu**

Insufficient bone formation and excessive bone resorption caused by estrogen deficiency are the major factors resulting in the incidence of postmenopausal osteoporosis (PMOP). The existing drugs usually fail to re-establish the osteoblast/osteoclast balance from both sides and generate side-effects owing to the lack of bone-targeting ability. Here, engineered cell-membrane-coated nanogels PNG@mR&C capable of scavenging receptor activator of nuclear factor-κB ligand (RANKL) and responsively releasing therapeutic PTH 1–34 in the bone microenvironment are prepared from RANK and CXCR4 overexpressed bone mesenchymal stem cell (BMSC) membrane-coated chitosan biopolymers. The CXCR4 on the coated-membranes confer bone-targeting ability, and abundant RANK effectively absorb RANKL to inhibit osteoclastogenesis. Meanwhile, the release of PTH 1–34 triggered by osteoclast-mediated acid microenvironment promote osteogenesis. In addition, the dose and frequency are greatly reduced due to the smart release property, prolonged circulation time, and bone-specific accumulation. Thus, PNG@mR&C exhibits satisfactory therapeutic effects in the ovariectomized (OVX) mouse model. This study provides a new paradigm re-establishing the bone metabolic homeostasis from multitargets and shows great promise for the treatment of PMOP.

1. Introduction

Osteoporosis is a common skeletal disorder characterized by decreased bone mass and deteriorated bone microarchitecture, accompanied by increased bone fragility and fracture risk.[1] In women, postmenopausal osteoporosis (PMOP) attributed to estrogen deficiency has become the commonest type, with about 50% of females suffering at least one fracture after menopause.[2]

As with other types of osteoporosis, the imbalance between osteoblastic bone formation and osteoclastic bone resorption is considered to be the immediate cause of PMOP.[3] In menopausal women, the expression of receptor activator of nuclear factor-κB ligand (RANKL) is increased, while its decoy receptor osteoprotegerin (OPG) is downregulated because of estrogen deficiency,[4] resulting in excessive activation of receptor activator of nuclear factor-κB (RANK) on the membrane of osteoclast precursors.[5] Then the

Y. Cui, D. Fu
Department of Orthopaedics
Shanghai Sixth People's Hospital Affiliated to Shanghai Jiao Tong University School of Medicine
Shanghai 200233, P. R. China
E-mail: fudehao@sjtu.edu.cn

B. Lv, Y. Geng, G. Liu
Union Hospital
Tongji Medical College
Huazhong University of Science and Technology
Wuhan, Hubei 430022, P. R. China

Z. Li, C. Ma
Department of Rehabilitation
Taihe Hospital
Hubei University of Medicine
Shiyan, Hubei 442000, P. R. China

Z. Gui
Department of Thyroid and Breast
Tongji Hospital of Tongji Medical College of Huazhong University of Science and Technology
Wuhan, Hubei 430030, P. R. China

L. Sang, X. Qi
Department of Orthopaedics
The Third Hospital
Hebei Medical University
Shijiazhuang, Hebei 050051, P. R. China
E-mail: qixiangbei126@126.com

C. Xu, Q. Min, Y. Liu
Department of Spine Surgery
Changzheng hospital
Naval Medical University
Shanghai 200003, P. R. China
E-mail: liuyangspine@hotmail.com

L. Kong, Z. Zhang
Tongji School of Pharmacy
Huazhong University of Science and Technology
Wuhan 430030, P. R. China

The ORCID identification number(s) for the author(s) of this article can be found under https://doi.org/10.1002/smll.202303494

DOI: 10.1002/smll.202303494

signaling adaptor tumor necrosis factor receptor (TNFR) associated factor 6 (TRAF6) is activated, thereby stimulating nuclear factor-κB (NF-κB) and mitogen-activated protein kinase (MAPK) pathway, and activating the osteoclast-related transcription factors (TFs), such as nuclear factor of activated T-cell cytoplasmic 1 (NFATc1).[4b,5] Due to the activation of these TFs and pathways, the transcription of osteoclastogenesis and bone resorption-related genes are initiated, mediating the bone loss eventually.[4b,5] Meanwhile, estrogen deficiency will impair the survival and mineralization capacity of osteoblasts,[6] which further aggravates the imbalance between excessive bone resorption and inadequate bone formation.

Given the importance of re-establishing the osteoblast/osteoclast balance, the present strategies for osteoporosis management mainly concentrate on promoting osteoblastic osteogenesis and suppressing osteoclastic activity. Synthetic parathyroid hormone (PTH) and RANKL-targeted antagonist denosumab are the first-line clinical medicaments aiming at osteoblasts and osteoclasts, respectively. Synthetic PTH, also known as recombinant human PTH 1–34 (the active 1–34 amino acid sequence of PTH), has been approved as the only osteoanabolic therapy of osteoporosis for many years. PTH 1–34 has been demonstrated to promote osteoblast differentiation and survival, thus improving bone microarchitecture and significantly reducing both limb and vertebra fracture rates.[7] However, PTH and synthetic PTH have also been proven to facilitate osteoclast formation and resorption activity via increasing the osteoblastic RANKL production,[8] thus the individual use of PTH 1–34 may not reconstruct the bone metabolic balance in osteoclast-dominant environment of PMOP patients. As for denosumab, it works as the RANKL scavenging antibody to suppress the osteoclast formation powerfully, for the modified antibody exhibits stronger neutralizing potency than natural OPG.[9] However, exorbitant osteoclast inhibition will also impair endogenous bone regeneration, as the sharp decline of released factors is embedded in the bone matrix during the resorptive process, which promotes osteogenesis and angiogenesis. In addition to the shortcomings mentioned above, these medications for osteoporosis suffer from common defects such as a lack of bone-targeting ability, side effects on other organs, and inadequate circulation time. Moreover, the intricate pathogenesis of osteoporosis regularly concerns multiple targets. Consequently, the separate osteoblast or osteoclast-target treatment is inadequate to recover the homeostasis in osteoporotic microenvironment. Therefore, developing a novel therapeutic multitarget system with specific targeting ability and long-circulation property is in urgent demand.

In recent decades, nanoparticles (NPs) coated with cell membranes have exhibited tremendous promise in precise treatment. The cell membrane that cloaked NPs can provide camouflage to protect NPs from clearance by the mononuclear phagocyte system, prolong the circulating time, reduce the immunogenicity and maximize the biocompatibility.[10] Moreover, some cell membrane-coated NPs conferred targeting ability and accumulated in specific tissues because of the various targeting moieties in the coated membranes.[10e,11] For instance, multiple myeloma cells coated NPs can enter the bone marrow and target the tumor cells via homologous targeting ability.[11a] Neutrophil-like cell membrane coated NPs have been reported to bind onto the inflamed brain microvascular endothelial cells and achieve active targeting drug delivery to the damaged brain.[11c] Besides the membrane targeting function, some membrane-coated NPs can absorb and clear pathological molecules such as cytokines,[12] antibodies, or toxins via the specific interactions with receptors on the membrane.[13] This neutralizing function has been described as nanodecoys in previous studies.[12a,b,13,14] For example, lipopolysaccharide-treated macrophage membrane-coated NPs have been developed to neutralize proinflammatory cytokines via the special affinity of the membrane receptors.[12c] In the treatment of PMOP, membrane-coated NPs with the ability to scavenge RANKL and TNF-α have been constructed to prevent osteoclastogenesis and promote osteogenesis,[12a] which enlighten us to utilize the membrane-coating technology to develop novel medication for the treatment of POMP. In addition to the advantages offered by membranes, the membrane-coated NPs usually load and delivery specific therapeutic molecules, which can be released in response to the acidity,[15] redox microenvironment and other physicochemical stimuli.[10e,16] If all the superiorities (membrane camouflage, targeting ability, neutralizing function and responsive release) of cell membrane-coated NPs are covered in one drug delivery system (DDS) for the POMP treatment, it may concurrently realize the bone-specific neutralization of pathological molecules, such as RANKL, and bone-targeted release of therapeutic drugs with responsiveness, thereby implementing the precise treatment of POMP at multitargets. However, the desirable system is still lacking according to our knowledge.

In this work, we engineered the mouse bone mesenchymal stem cells (BMSCs) to overexpress the C-X-C motif chemokine receptor 4 (CXCR4) and RANK on their membrane. The membrane of these engineered BMSCs was then extracted and coated on pH-sensitive chitosan-based nanogels containing PTH 1–34, to construct biomimetic nanogels PNG@m&C. The abundant membrane CXCR4 conferred these nanogels bone-targeting ability, and the RANK endowed them with RANKL-absorbing ability. When PNG@m&C was administrated, the bone-targeting ability could facilitate its accumulation in the bone microenvironment. The osteoclast-mediated acid microenvironment could contribute to the PTH 1–34 release owing to the pH-responsive property of biomimetic nanogels,[17] and the released PTH 1–34 will promote osteogenic differentiation and bone formation. Meanwhile, the overexpressed RANK protein on the membrane constituents neutralized RANKL to relieve the excessive osteoclast formation. Thus, the PNG@m&C may represent a novel multitarget therapeutic system for PMOP.

2. Results and Discussion

2.1. Preparation and Characterization of PNG@mR&C

The preparation of PNG@mR&C briefly comprised two steps: obtaining genetically engineered BMSC-membrane vesicles mR&C and followed by enveloping mR&C onto the PTH 1–34 containing nanogels (**Figure 1**A). The engineered membrane involved two particular proteins, RANK and CXCR4. RANK, also known as TNFRSF11A, belonged to the type I membrane protein and was the only known signaling receptor for RANKL.[18] The membrane of cells expressing RANK such as RAW 264.7

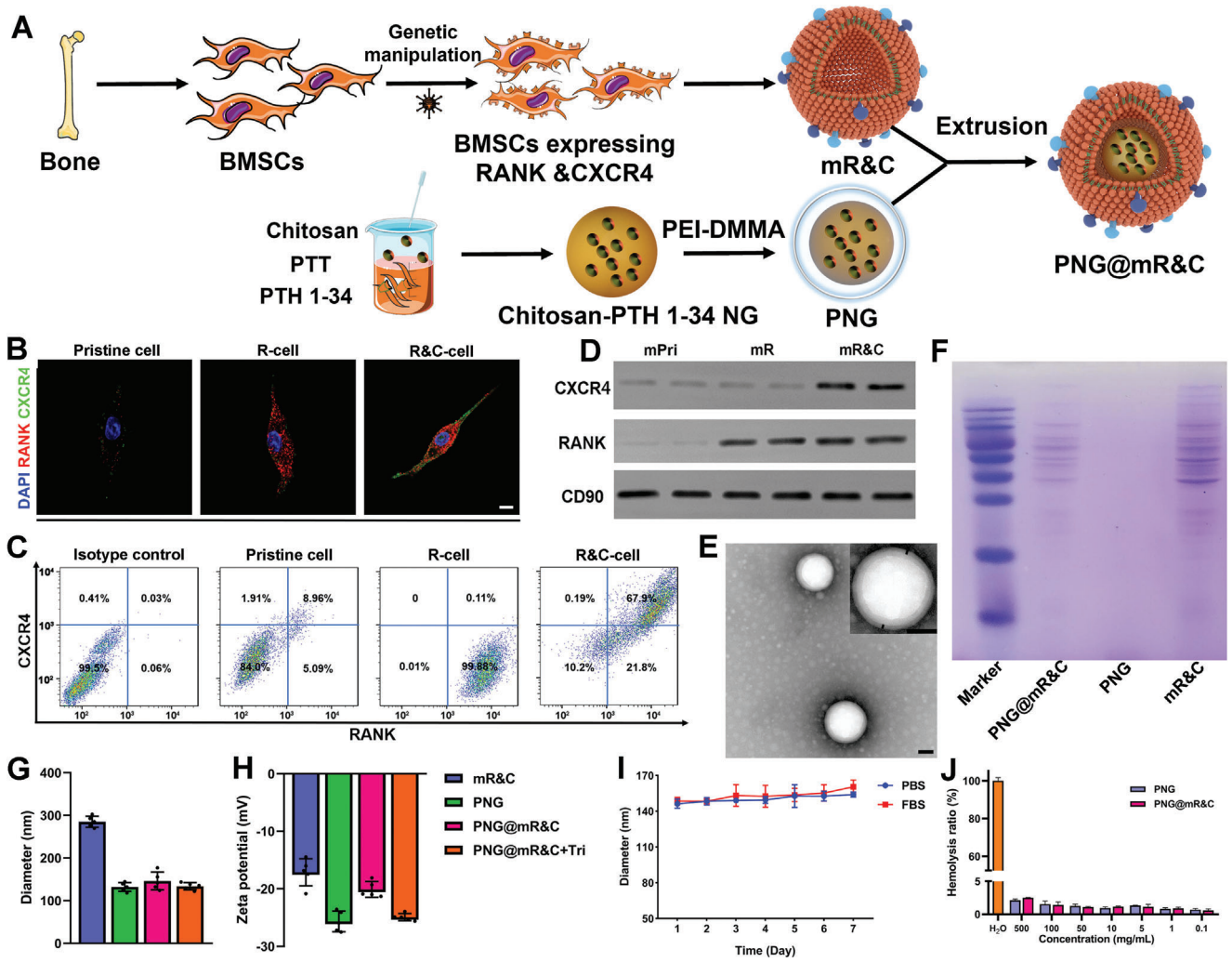

Figure 1. Preparation and characterization of engineered cells and PNG@mR&C. A) Schematic illustration of PNG@mR&C preparation. B) Representative immunofluorescence images of bone mesenchymal stem cells (BMSCs) labeled with RANK and CXCR4 antibodies. 4′,6-Diamidino-2-phenylindole (DAPI) was used to show nucleus. Scale bar = 10 μm. C) Flow cytometry (FCM) analysis of RANK and CXCR4 expression on the pristine and genetically engineered BMSCs. D) Western blotting analysis of RANK and CXCR4 expression in the extracted membrane from the pristine BMSCs (mPri), RANK-overexpressed BMSCs (mR) and RANK and CXCR4-overexpressed BMSCs (mR&C). E) Transmission electron microscopy (TEM) photograph of PNG@mR&C. Scale bar = 50 nm. F) Sodium dodecyl sulfate-polyacrylamide gel electrophoresis (SDS-PAGE) analysis of PNG@mR&C, PNG, and mR&C. G,H) Hydrodynamic diameter and zeta potential of mR&C, PNG, PNG@mR&C, and PNG@mR&C treated with Triton X-100 (PNG@mR&C + Tri) ($n = 5$). I) Hydrodynamic diameter variation of PNG@mR&C in phosphate buffer saline (PBS) and fetal bovine serum (FBS) ($n = 5$). J) Hemolysis test of PNG@mR&C and PNG ($n = 3$).

had been developed as scavenging agents for RANKL to treat osteoporosis.[12a] However, these membranes were not adopted here because of the potential safety risk and lacking bone-targeting ability when tumor-derived RAW 264.7 cell line was used.[19] Another crucial protein, CXCR4, acted as the receptor of stromal cell-derived factor1 (SDF1, also termed as C-X-C motif chemokine 12), which was abundant in the bone marrow.[20] The surface display of CXCR4 on NPs or exosomes had been proven to increase their distribution in bone.[21] Herein, the RANK and CXCR4 were transduced onto murine BMSCs by lentivirus step by step. We demonstrated the RANK and CXCR4 expression on BMSCs by immunofluorescence and flow cytometry (FCM) (Figure 1B,C). Although these proteins were reported to be expressed on pristine BMSCs under certain conditions,[22] the natural expression was not adequate to realize the RANKL clearance or bone targeting effects. Then the cell membrane components were obtained using the commercial kits reported in our previous study.[15a] Subsequently, the retention of RANK and CXCR4 on the extracted membrane was confirmed with Western blotting (Figure 1D). Ultimately, the PNG@mR&C was prepared with sonication and successive extrusion. The morphology of PNG@mR&C presented a typical core-shell structure under transmission electron microscopy (TEM) (Figure 1E). Sodium dodecyl sulfate-polyacrylamide gel electrophoresis (SDS-PAGE) assay was conducted to detect the protein contents of membrane-coated nanogels and the results manifested PNG@mR&C retained the protein content of RANK and CXCR4-overexpressed BMSC membrane (mR&C) (Figure 1F). Moreover, the sizes

and zeta potentials of PTH 1–34 containing nanogel (PNG), PNG@mR&C, and PNG@mR&C treated with Triton X-100 (a membrane breaking reagent) were measured with dynamic light scattering (DLS) (Figure 1G,H; Figure S1, Supporting Information). As shown in Figure 1G,H, the mean diameter and zeta potential of PNG were 132.3 ± 9.2 nm and −25.6 ± 1.6 mV, respectively. After membrane coating manipulation, the size and zeta potential of PNG@mR&C increased to 146.3 ± 18.7 nm and −20.1 ± 1.2 mV, respectively. Zeta potential was related to the surface charge of NPs. Since cellular membranes were mostly negatively charged, cationic NPs (potentials greater than +30 mV) usually displayed cytotoxicity associated with membrane disruption. Both PNG and PNG@mR&C showed negative zeta potential, which could avoid the cytotoxicity. When PNG@mR&C was treated with Triton X-100, the diameter and zeta potential decreased markedly to 133.9 ± 7.6 nm and −24.9 ± 0.6 mV, close to those values of PNG. These results further indicated the membrane was coated onto PNG successfully.

Then the stability, safety, encapsulation efficiency (EE), and drug loading capacity (DLC) of PNG@mR&C were investigated in the following study. The particle size variation of PNG@mR&C was monitored in phosphate buffer saline (PBS) or PBS containing 20% fetal bovine serum (FBS) for 7 days. In both solutions, the PNG@mR&C exhibited good stability with a very slightly changed diameter (Figure 1I). The cytotoxicity and safety of PNG@mR&C were evaluated with Cell Counting Kit-8 (CCK-8) assay and hemolysis test in vitro. Both NG and NG@mR&C containing no PTH 1–34 showed negligible cytotoxicity up to the tested concentration of NG at 500 mg mL^{-1}. After loading with PTH 1–34, PNG and PNG@mR&C exhibited a prosurvival effect on pre-osteoblasts, which was consistent with the previous report (Figure S2, Supporting Information).[23] The hemolysis assay results also showed negligible hemolysis (<5%) of PNG@mR&C and PNG in all concentrations (Figure 1J), which demonstrated that this system possessed good biosafety. Then the EE of PTH 1–34 was determined under different feeding amounts as reported in our previous study,[15a] which manifested the EE remained over 95.07% when 2.5 μg PTH 1–34 was fed into 50 μg nanogels (Figure S3, Supporting Information). At this feeding amount, the DLC was 4.06 μg per 100 μg PNG@mR&C, which indicated the chitosan biopolymer possessed desired loading capacity of polypeptide.

2.2. Bone-Targeting Ability and pH-Responsiveness of PNG@mR&C

Although CXCR4 modification had been accepted to increase bone-specific accumulation,[21] the bone-targeting ability of PNG@mR&C was further confirmed in this study. Nanogels coated by different membrane were labeled with lipophilic DiR fluorescent dye and injected into mice. Then the major organs were collected after different time and detected under biophotonic imaging system. As displayed in **Figure 2**A, little fluorescence was detected in brain, heart, spleen, lung and kidney at 8 h after injection, while fluorescence in the liver still maintained at a high intensity. This observation was in accordance with the previous study,[21a] which was probably because the main metabolic process of these NPs occurred in liver. PNG@mR&C group exhibited stronger fluorescence intensity in the femur but weaker fluorescence intensity in liver than PNG@mR group (only RANK-overexpressed membrane coated nanogels), which indicated that CXCR4 overexpression could increase the bone accumulation and reduce the nonspecific distribution. To further validate whether the bone-targeting ability was CXCR4-dependent, PNG@mR&C were pre-treated with CXCR4 antibody to occupy the CXCR4 protein. As expected, antibody preincubation attenuated the fluorescence intensity (Figure 2B). These results demonstrated that PNG@mR&C possessed the CXCR4-dependent bone-targeting ability. In addition, the bone-specific distribution of PNG@mR&C was still high at 8 h after administration. Speculatively, the circulating time of PNG@mR&C was much longer than the current PTH 1–34 Teriparatide injection, which only possessed a half-life of 1 h.

Albeit SDF-1 was expressed in many tissues, higher levels of SDF-1 was proved to exist in the bone marrow and liver compared to other organs. Thus, the experimental data demonstrated that PNG@mR&C distribution was huge in liver. Then we analyzed the fluorescence distribution proportion of PNG@mR&C in these major organs, which could reflect the affinity of PNG@mR&C to other organs. At 4 h, the distribution proportion ranking from high to low were: liver (56.3%), lung (18.6%), femur (15.8%), kidney (2.7%), brain (2.3%), heart (2.2%), and spleen (2.2%). At 8 h, the distribution proportion ranking from high to low were: liver (66.8%), femur (25.7%), spleen (2.1%), lung (1.5%), kidney (1.5%), heart (1.4%) and brain (0.9%) (Figure S4, Supporting Information). These data may indicate the relative targeting ability of PNG@mR&C to different organs. Among these organs, liver had both rich blood supply and SDF-1 expression, thus it exhibited most extensive accumulation of PNG@mR&C at both 4 and 8 h. The lung showed an abundant PNG@mR&C distribution at the initial time probably because its rich blood. However, the accumulation got very little due to lacking of SDF-1 expression and low active targeting ability, which could be further investigated in the future. Although femur was relatively lacking of blood supply compared to liver and lung, it showed relatively abundant PNG@mR&C distribution, which further demonstrated PNG@mR&C possessed available active bone-targeting ability.

In addition to bone-targeting ability, the nanogel enveloped in PNG@mR&C was designed with the property of rapid degradation in a slightly acidic microenvironment, due to the pH-responsiveness of outside dimethyl maleic anhydride modified polyethyleneimine (PEI-DMMA) component in the nanogel.[24] As proved in our previous study,[15a] the hydrophobic PEI-DMMA layer at neutral pH would be protonated and switched to hydrophilic under pH 6.5. It was accepted that the local microenvironment around mature osteoclasts was acidic as they secreted numerous hydrogen ions (H^+) for bone resorption.[5,17] The regional acidic environment could serve as a trigger for the rapid drug release from the nanogels.

To investigate the pH-responsiveness of PNG@mR&C, the transmittance of PNG@mR&C dispersed in PBS was measured when the pH value of the systems was adjusted from 7.9 to 6.4. In neutral and alkalescent environment, the PNG@mR&C solution was stable colloidal suspension, thus it was nontransparent unless degraded. As manifested in Figure 2C, the PNG@mR&C solution remained a stable transmittance value of around 0% up

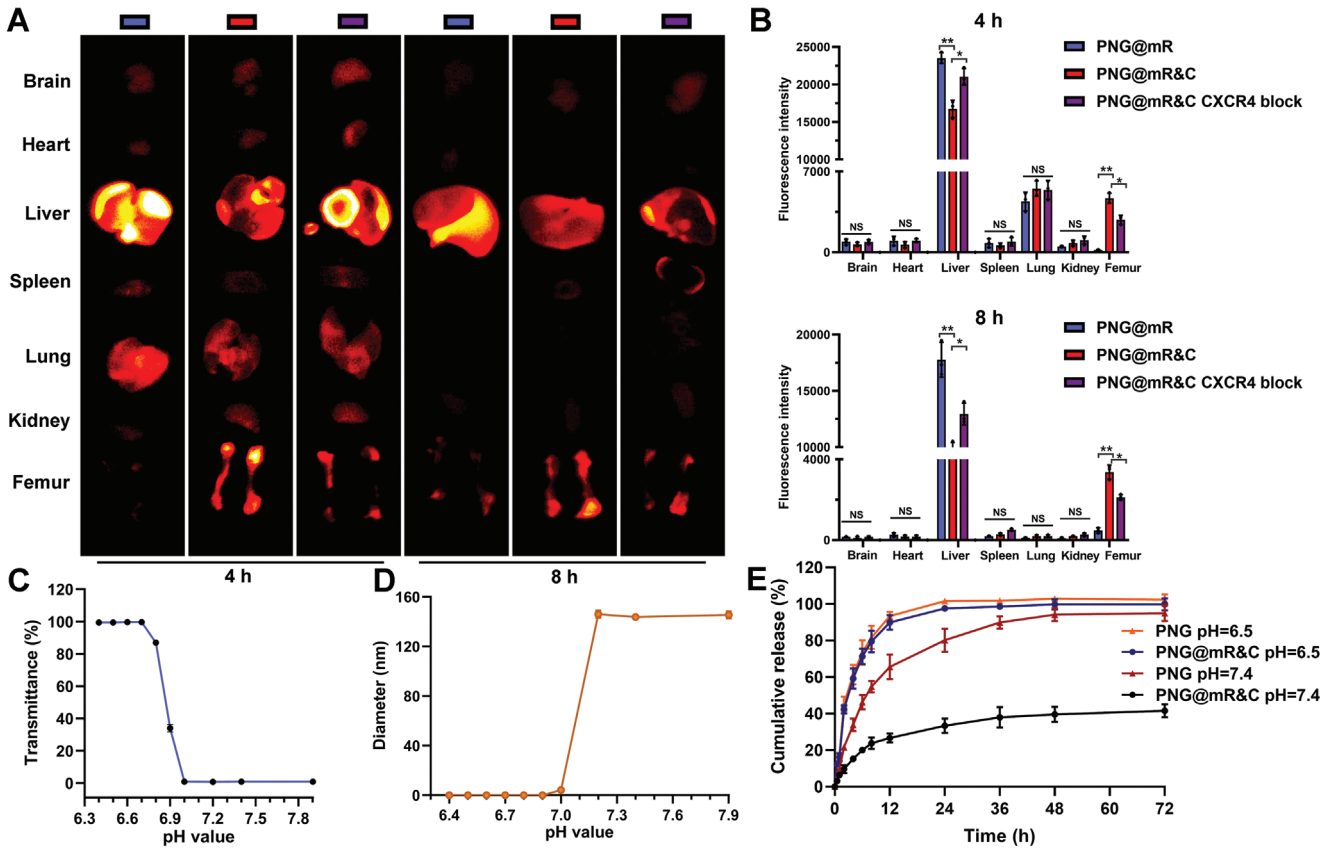

Figure 2. Bone-targeting ability and pH-responsiveness of PNG@mR&C. A) Biodistribution of the DiR-labeled PNG@mR&C at 4 and 8 h in mice. B) Quantification of fluorescence intensity at 4 and 8 h in different organs ($n = 3$). (NS, no significant difference; $^{*}p < 0.05$; $^{**}p < 0.01$). C) The transmittance of PNG@mR&C solution at various pH values ($n = 3$). D) The diameter changes of PNG@mR&C at various pH values ($n = 3$). E) The cumulative release of PTH 1–34 from PNG and PNG@mR&C at 37 °C under pH = 7.4 or 6.5 ($n = 3$).

to pH 7.2, while the transmittance suddenly became 90% around pH 6.7, which indicated that the nanogels were degraded in a slightly acidic environment. Furthermore, the particle sizes of PNG@mR&C at different pH conditions were measured using DLS. As shown in Figure 2D, the PNG@mR&C remained relatively stable under physical pH environment but dramatically vanished in acidic environments, which could also demonstrate the pH-responsive degradation of nanogels.

Then we determined the drug release property of PNG@mR&C which were dispersed in PBS at pH 7.4 and 6.5 to mimic the blood and bone resorption microenvironment, respectively. As shown in Figure 2E, there was only 26.6% of PTH 1–34 released from PNG@mR&C at pH 7.4 in the first 12 h, and the slow release lasted until 72 h, which indicated that the system possessed a good drug retention capability and stability under normal physiological conditions. Whereas, the release of PTH 1–34 was much faster at pH 6.5. The cumulative release profiles manifested that 89.8% of PTH 1–34 was released under the slightly acidic environment in the initial 12 h. The release property of PNG@mR&C was similar to another membrane-enveloped PEI-DMMA-coated nanogels in our former study.[15a] The protonation of PEI-DMMA mediated by acidic conditions contributed to the swelling of chitosan nanogel core, and the consequent disruption of membrane coated structure. After the disassembling of the membrane and PEI-DMMA layer, the loaded PTH 1–34 was released eventually. Thus, the influence of the membrane coating on the release of PTH 1–34 from PNG@mR&C was further investigated. As shown in Figure 2E, the PTH 1–34 released from PNG@mR&C was much lower than that from PNG in the initial 12 h at pH 7.4, which indicated that the membrane coating could effectively reduce the off-target release or leakage in the normal physiological environment. However, the releasing profile of PNG was similar to that of PNG@mR&C, which suggested that the membrane coating could not prevent the protonation of the PEI-DMMA layer in the acidic environment. The above results manifested that PNG@mR&C could effectively realize the delivery of PTH 1–34 with pH responsiveness and reduce the leakage in blood circulation.

2.3. PNG@mR&C Scavenged RANKL and Inhibited Osteoclastogenesis In Vitro

The PNG@mR&C-mediated RANKL scavenging effect was first investigated by detecting the concentration of remaining RANKL after the NPs were incubated in RANKL solution for 2 h. Pristine BMSC membrane-coated nanogels (PNG@mPri) were prepared

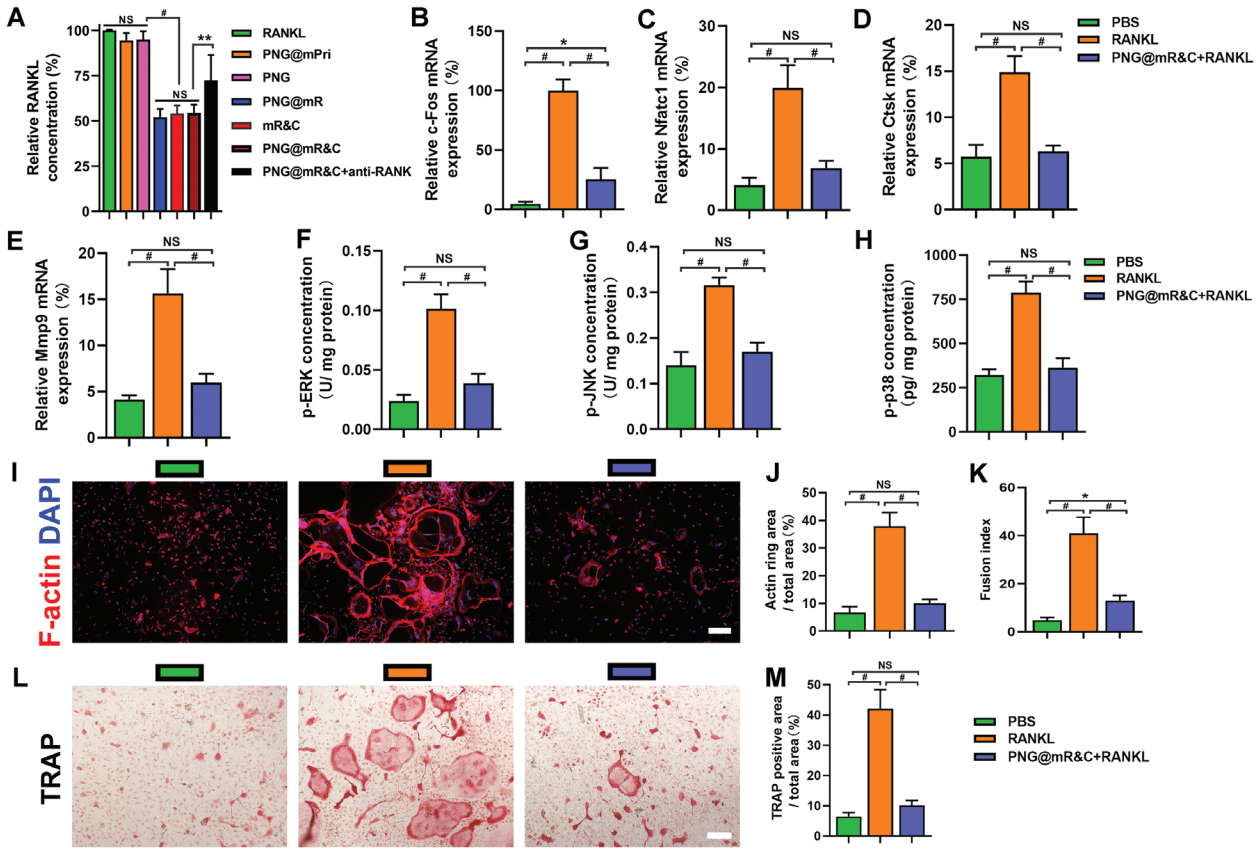

Figure 3. PNG@mR&C scavenged receptor activator of nuclear factor-κB ligand (RANKL) and inhibited osteoclastogenesis in vitro. A) Relative RANKL concentration in the remaining solutions after treatment with PNG@mPri, PNG, PNG@mR, mR&C, PNG@mR&C, and RANK antibodies preincubated PNG@mR&C (PNG@mR&C + anti-RANK) ($n = 3$). B–E) Relative mRNA expression of c-Fos, Nfatc1, Ctsk, and Mmp9 gene. F–H) Quantitation of p-ERK, p-JNK, and p-p38 concentration in bone marrow macrophages (BMMs) when PNG@mR&C was used to intervene the RANKL-mediated osteoclast formation ($n = 3$). I) Representative photographs of F-actin staining assay. Scale bar = 100 μm. J) Quantitation of F-actin ring areas ($n = 3$). K) Quantitation of fusion index ($n = 3$). L) Representative images of tartrate-resistant acid phosphatase (TRAP) staining. Scale bar = 100 μm. M) Quantitation of the TRAP-positive areas ($n = 3$). (NS, no significant difference; $^{*}p < 0.05$; $^{**}p < 0.01$; $^{\#}p < 0.0001$).

as a negative control. As shown in **Figure 3**A, PNG@mR&C-mediated distinct and concentration-dependent RANKL scavenging effect (Figure S5, Supporting Information). Parallel with PNG@mR&C, the PNG@mR and mR&C membrane vesicles also exhibited similar RANKL scavenging ability. In comparison, neither PNG@mPri without overexpressed RANK protein nor anti-RANK pre-incubated PNG@mR&C showed an obvious RANKL scavenging effect. These results indicated that the elimination of RANKL was dependent on the overexpressed RANK on the membrane.

Next, the PNG@mR&C-mediated anti-osteoclastogenesis effect was evaluated by examining the c-Fos, Nfatc1, matrix metalloproteinase (Mmp) 9, cathepsin K (Ctsk) mRNA expression during the PNG@mR&C-intervened osteoclastogenesis process of bone marrow macrophages (BMMs). As illustrated in Figure 3B, PNG@mR&C remarkably downregulated the expression of c-Fos, approaching the level of BMMs without induction of osteoclastogenesis. As the process of osteoclastogenesis induction progressed, the expression of Nfatc1, Mmp9, and Ctsk were also apparently downregulated (Figure 3C–E). In addition, PNG@mR&C significantly inhibited the phosphorylation of some kinases in MAPK pathways including extracellular signal-regulated kinase (ERK), c-Jun N-terminal protein kinase (JNK) and p38 (Figure 3F–H). The phosphorylation of them was recognized to be crucial for normal osteoclast formation and activation. Therefore, PNG@mR&C could disturb the RANKL-induced activation of the osteoclastogenesis-related pathway.

Furthermore, the osteoclast differentiation of BMMs was investigated after PNG@mR&C intervention. Similar to the inhibition of c-Fos and MAPK pathways, and F-actin staining results (Figure 3I,J) exhibited that the osteoclast formation of BMMs was notably impaired by PNG@mR&C and the fusion index (defined as the means of nuclei number per osteoclast) (Figure 3K) was remarkably reduced.[25] The tartrate-resistant acid phosphatase (TRAP) staining results (Figure 3L,M) also showed that PNG@mR&C inhibited the osteoclastogenesis of BMMs.

2.4. PNG@mR&C Promoted Osteogenesis In Vitro

The PNG@mR&C was designed with the loading of PTH 1–34 to promote osteogenesis. Theoretically, PTH 1–34 could be responsively released in the osteoclast-mediated regional acidic environment in vivo. To mimic this microenvironment, pre-osteoblasts

and osteoclasts coculture experiments were conducted using a transwell plate (**Figure 4**A). The previously formed osteoclasts were reseeded on the upper chamber, and the pre-osteoblast MC3T3-E1 cells were cultured in the lower chamber for osteogenic differentiation induction. When PNG@mR&C was incubated with osteoclasts in the upper chamber, the concentration of PTH 1–34 increased markedly (Figure S6, Supporting Information). Due to the released PTH 1–34, pre-osteoblasts showed a remarkably increased cyclic adenosine monophosphate (cAMP) production (Figure S7, Supporting Information), indicating the PTH receptor-related pathway was activated. As a contrast, the concentration of PTH 1–34 and cAMP production were much lower when PNG@mR&C was incubated without osteoclasts. These results also verified that the drug release of PNG@mR&C was acid-triggered. Then the pre-osteoblasts were conducted osteogenic differentiation induction under the influence of the upper chamber. Firstly, the expression of osteogenesis-related genes was detected to confirm the pro-osteogenic effects of PNG@mR&C at various time points of the differentiation process. As shown in Figure 4B, the expression of osteogenesis-related genes exhibited no significant difference in PNG@mR&C without osteoclast coculture compared with the control, while PNG@mR&C treatment under osteoclast coculture condition promoted the expression of Runt-related transcription factor 2 (Runx2), Osterix (Osx), Alkaline phosphatase (Alp), and collagen type alpha 1 (Col1a) at Day 3. These genes were usually initiated at the early stage of osteogenic differentiation. As the process of differentiation prolonged and fresh PNG@mR&C was supplemented every 3 days, the gene indicators of the early stage also increased in other groups. Whereas the expressions of osteocalcin (Ocn) and osteopontin (Opn) were still much lower than PNG@mR&C + OCs group at Day 14. These results indicated that the process of osteogenic differentiation was accelerated by the osteoclast-triggered PTH 1–34 release from PNG@mR&C. Besides this, the expression of the OSX and OCN proteins was investigated using immunofluorescence staining at Day 3, Day 7 and Day 14 (Figure 4C). The results were in accord with the expression of osteogenesis-related genes (Figure 4D,E). In addition to the gene and protein aspects, the pro-osteogenic effects of PNG@mR&C were evaluated with ALP and Alizarin red S (ARS) staining. These results (Figure 4F–I) also showed that the ALP activity and mineralized nodule formation were increased in PNG@mR&C + OCs group. Collectively, these results manifested that PNG@mR&C could remarkedly promote the osteogenesis of pre-osteoblasts via releasing PTH 1–34 pH-responsively.

2.5. Anti-Osteoporosis Effects of PNG@mR&C in OVX Mice

The anti-osteoporosis efficacy of PNG@mR&C was evaluated in bilateral ovariectomized (OVX) mimic PMOP mouse models after they were intravenously administrated every 3 days for 8 weeks (**Figure 5**A). As the gold-standard technology for assessing the three-dimensional bone morphology of small animals, micro-computed tomography (micro-CT) can be used to accurately and visually evaluate the bone microstructure.[26] As demonstrated in Figure 5B, the OVX-mediated bone loss was alleviated after treatment of PNG@mR&C, and the PNG@mR&C administration even showed more bone mass gain than the direct PTH 1–34 administration. The bone microarchitecture parameters including bone mineral density (BMD), trabecular bone volume/total volume (Tb. BV/TV), trabecular number (Tb. N), and trabecular separation (Tb. Sp) were largely improved after PNG@mR&C treatment (Figure 5C–F). In addition to micro-CT-derived bone morphometry and density measurements, the mechanical strength of the load-bearing bones was also critical to reflect the therapeutic effects. The three-point bending test manifested that the mechanical strength of tibia was distinctly improved after PNG@mR&C administration (Figure 5G,H).

The above assays proved the favorable effects of PNG@mR&C on bone mass and mechanical property recovery. Besides these, the rebalance of osteoblast and osteoclast in osteoporotic microenvironment was also noteworthy. The mineral apposition rate (MAR) reflected the deposition and mineralization rate of osteoid matrix produced by osteoblast;[27] thus, this indicator can represent the activity of mature osteoblast. As illustrated in **Figure 6**A,B, the bone-targeted delivery of PTH 1–34 by PNG@mR&C showed higher MAR than conventional PTH 1–34 administration. Moreover, the OCN immunofluorescence staining of bone tissue was conducted, and the expression of OCN was markedly increased after PNG@mR&C treatment (Figure 6C,D). Whereafter, the TRAP staining was conducted to investigate the activity of osteoclasts in vivo. Due to the OVX operation and the resultant estrogen deficiency, the osteoclasts were remarkably increased. Although it showed increased osteoblast mineralization after PTH 1–34 administration, the osteoclasts-mediated bone resorption was also promoted in vivo (Figure 6E,F). This phenomenon was in accordance with the conclusion of previous study in which intermittent PTH provoked increased RANKL expression and the resulting increase of osteoclastic resorptive activity.[23,28] Dialectically speaking, the PTH 1–34 mediated osteoclastic promotion would result in the release of growth factors favoring osteogenesis from the matrix, and these factors were an additional source of pro-osteogenic signals contributing to the bone anabolism effect.[23,28b] Therefore, the ultimate effect of PTH 1–34 was gain of bone mass. However, this effect could be improved if the pro-resorptive function of PTH 1–34 were avoided in the exorbitant bone resorption microenvironment of PMOP patients. To realize the proper reservation of pro-osteogenic factors mediated by bone resorption and refrainment of the further bone catabolism mediated by PTH 1–34, the PNG@mR&C administration showed more satisfactory effect. As exhibited in Figure 6E,F, the osteoclasts activity of PNG@mR&C group was close to that of normal mice. As for NG@mR&C administration, it also realized the decrease of osteoclast activity but failed to promote osteogenesis.

To further confirm the rebalance of osteoblast and osteoclast after PNG@mR&C treatment, the assays of molecular level were conducted. Firstly, the serum RANKL and OPG concentrations of different groups were measured. Compared to the control group, the RANKL in NG@mR&C and PNG@mR&C-treated OVX mice remarkably decreased, nearly close to the normal levels. However, the PTH 1–34 administration slightly increased RANKL concentration in the serum (Figure 6G), which was consistent with the previous report.[23] The OPG and estradiol concentrations of each groups showed no significant difference (Figure S8, Supporting Information). Beyond these, serum biochemical markers of bone turnover were also examined from the metabolic aspect,

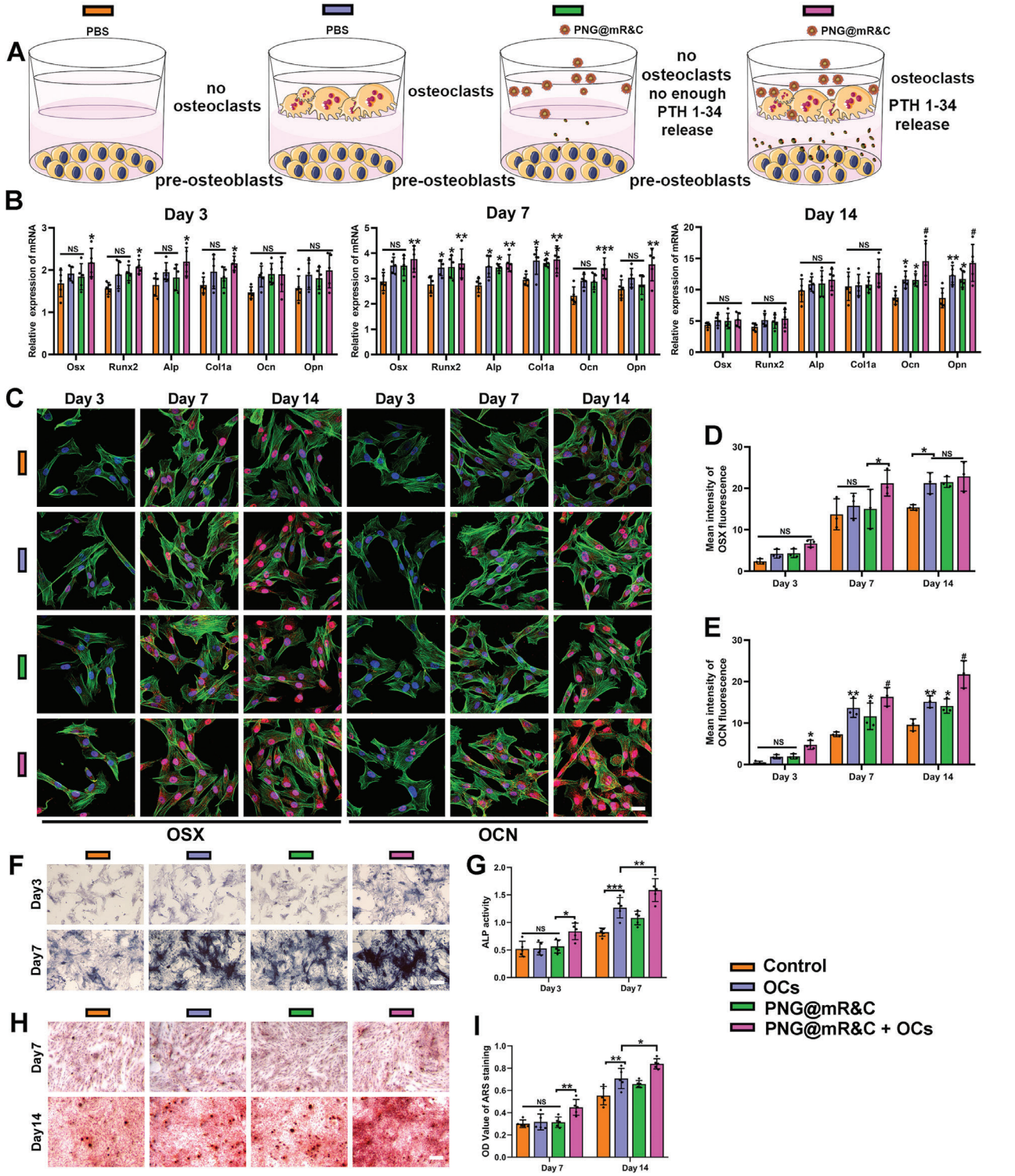

Figure 4. PNG@mR&C promoted osteogenesis in vitro. A) Schematic illustration about treatment of different groups. B) Relative mRNA expression of osteogenesis-related genes (Osx, Runx2, Alp, Col1a, Ocn, and Opn) at Days 3, 7, and 14 in different groups during the osteogenic induction process ($n = 5$). C) Representative images showing immunofluorescence staining of osteogenic differentiation-related proteins OSX and OCN after different treatment at Days 3, 7, and 14. Green fluorescence represents FITC-phalloidin, and the red fluorescence represents the OSX or OCN. Scale bar = 20 µm. D,E) Quantitative analyses of the OSX and OCN fluorescence staining ($n = 3$). F) Representative photographs of ALP staining during the osteogenic differentiation process. Scale bar = 100 µm. G) ALP activity of pre-osteoblasts in different groups ($n = 5$). H) Representative photographs of ARS staining during the osteogenic differentiation process. Scale bar = 100 µm. I) Quantitative analysis of ARS staining ($n = 5$). (NS, no significant difference; $^{*}p < 0.05$; $^{**}p < 0.01$; $^{***}p < 0.001$; $^{\#}p < 0.0001$).

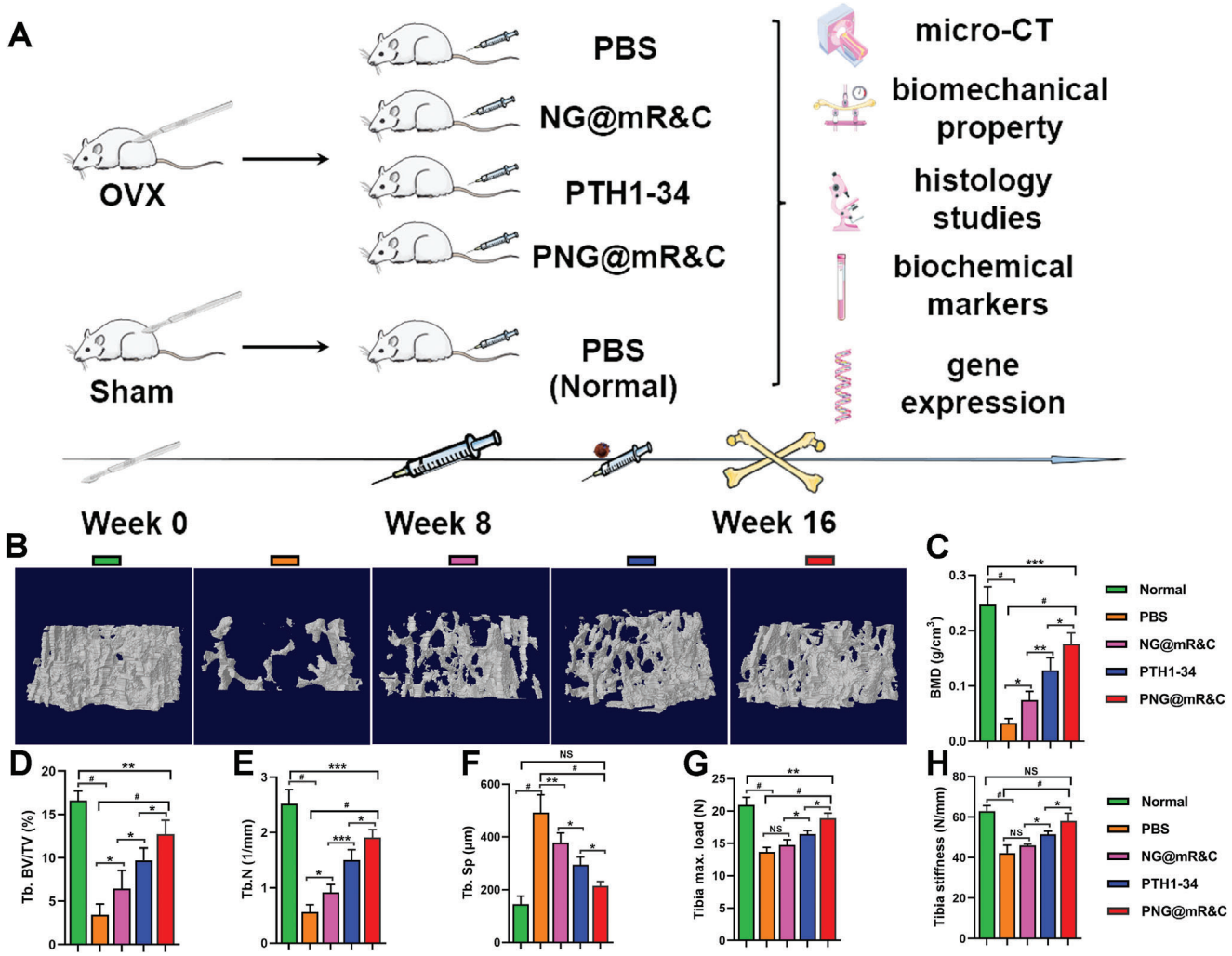

Figure 5. Anti-osteoporosis effects of PNG@mR&C in OVX mic. A) Schematic illustration of animal model in this study. B) Representative 3D reconstructed microcomputed tomography (micro-CT) images of bone microarchitecture in the distal femurs. C–F) Quantitative analysis of bone mineral density (BMD), Tb. BV/TV, Tb. N and Tb. Sp ($n = 5$). G,H) Quantitation of bone mechanical strength including the maximum load and stiffness of tibia by three-point bending measurement ($n = 5$).

including the concentrations of bone alkaline phosphatase (BAP), OCN, procollagen type-1 N-terminal propeptide (P1NP), tartrate resistant acid phosphatase 5b (TRAP5b), and β-isomerized carboxy-terminal telopeptides (β-CTX). Among these markers, TRAP5b and β-CTX, the degradation products of collagen fibres or the osteoclast-derived enzymes, were closely associated with bone resorption. BAP, OCN, and PINP, as byproducts or enzymes of osteoblasts or osteocytes during osteogenesis were closely related to bone formation.[29] After PNG@mR&C administration, these markers were recovered close to the normal mice (Figure 6H–L). Furthermore, the mRNA expressions of critical factors associated with osteogenic differentiation, osteoclastogenesis, RANKL/RANK/OPG system, and bone resorption activity of bone tissues were detected. As shown in Figure 6M, the critical genes involving osteogenic differentiation were compensated after PNG@mR&C administration. The excessive expressions of crucial osteoclast-related TFs (c-Fos and Nfatc1) and osteoclast-specific genes (Trap and Ctsk) were also restrained by PNG@mR&C treatment. The imbalance of RANKL/RANK/OPG system-related gene expression (Rankl, Rank, and Traf6) was rebalanced. Meanwhile, the genes involving bone resorption activity (Mmp2, Mmp9, and Mmp13) were decreased to the similar levels as normal mice, which would contribute to the net increase of bone mass (Figure 6N). Overall, the PNG@mR&C treatment showed more reasonable osteoblast/osteoclast balance compared to other groups (Figure 6O).

In addition, the blood routine examination demonstrated that there were no statistic differences of blood cell counts and percentages between PNG@mR&C treated and normal mice (Table S1, Supporting Information). The blood biochemistry analyses [including serum creatinine (Scr), blood urea nitrogen (BUN), total bilirubin (TBil), alanine aminotransferase (ALT) and aspartate aminotransferase (AST)] also manifested the mice possessed normal hepatorenal function after PNG@mR&C ministration (Figure S9, Supporting Information). Besides these, H&E staining of main organs (including heart, liver, spleen, lung, and

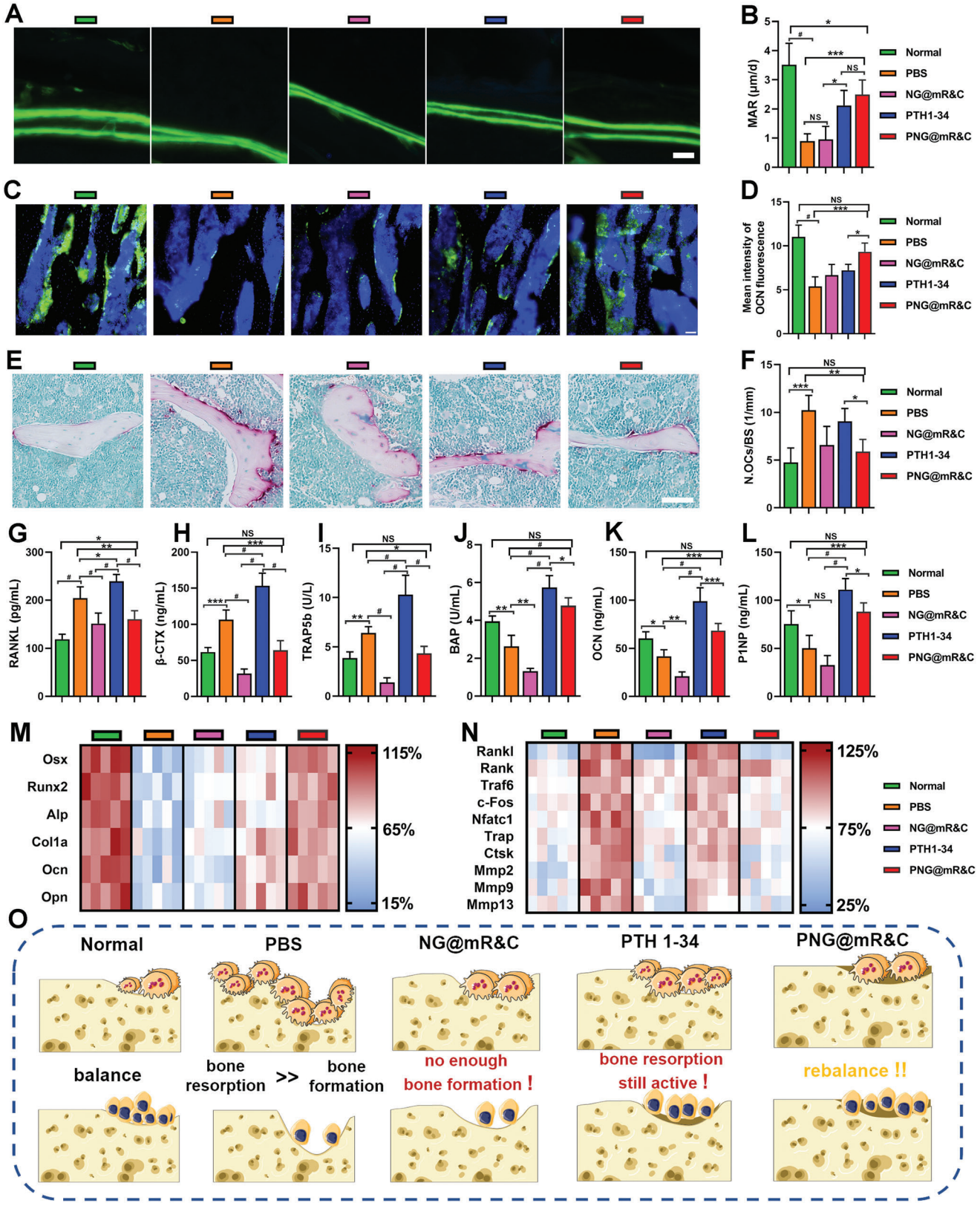

kidney) sections were conducted, and no pathologic changes were observed in each group (Figure S10, Supporting Information). All these results indicated that the PNG@mR&C treatment was of good safety.

3. Conclusions

In summary, engineered cell-membrane-coated nanogels with bone-targeting ability were constructed to specifically scavenge the RANKL and release PTH 1–34 in the bone microenvironment for the treatment of PMOP in this study. PNG@mR&C showed distinct advantages over those existing drugs which lacked the bone-targeting ability and failed to act on both osteoblasts and osteoclasts. Compared to the other NPs treating PMOP, the bone-specific RANKL neutralization of PNG@mR&C avoided the potential side effects owing to disturbing the normal physiological function of RANKL beyond bones. Meanwhile, the dose and frequency were much reduced due to the pH-responsive drug release, prolonged circulation time, and bone-targeting accumulation. Overall, PNG@mR&C realized the bone-specific neutralization of RANKL and bone-targeted release of anabolic drugs with smart responsiveness, which may provide a new paradigm for the treatment of PMOP. Of course, there are still some disadvantages of PNG@mR&C. Firstly, the preparation technology of PNG@mR&C was complicated and high-cost, thus it was still worth exploring the standardized technological process to accomplish the scale production. Secondly, the storge condition was still relatively harsh as the current commercial PTH 1–34 injection which need low temperature preservation, which increased the cost and reduced the convenience. Thirdly, the administration route was not the most comfortable. The inhalation administration was practicable in the treatment of PMOP, such as Salmon Calcitonin Nasal Spray, Novartis Pharma Schweiz AG, which was more convenient than the intravenous injection of our PNG@mR&C. In the near future, we will also try to develop the inhalation dosage form of PNG@mR&C and overcome the above disadvantages.

4. Experimental Section

BMSCs and BMMs Isolation and Induction: This work isolated and characterized the murine BMSCs from C57BL/6J (female, 8 weeks) mice as reported in previous studies. After sacrificed, the mice were sterilized with 75% alcohol and the bone marrow was flushed out through the femur and tibia with PBS. Then the flushed cells were cultured in mouse BMSC growth medium (CM-M131, Procell Life Science & Technology, Wuhan, China). The cells were cultured for proliferation, and they were used at passages 2 or 3 for the following assays. Surface protein markers [positive markers: CD73 (bs-4834R, Bioss, Beijing, China), CD90 (A23333, ABclonal Technology, Wuhan, China) and CD105 (E-AB-F1233C, Elabscience, Wuhan, China); negative markers: CD34 (A23108, ABclonal Technology) and CD45 (E-AB-F1136UF, Elabscience)] were detected with a flow cytometer (Beckman Coulter, USA). Osteogenic, chondrogenic and adipogenic differentiation experiments were conducted to confirm the multidifferentiation potentials of murine BMSCs. Murine BMMs were acquired as previously reported.[30] Briefly, the bone marrow cells were flushed out and cultured in α-modified Eagle's medium (α-MEM) containing 10% FBS (HB-FBS-50, HAKATA, Shanghai, China) and macrophage colony-stimulating factor (M-CSF) (30 ng mL^{-1}, MOP2225, KMD Bioscience, Tianjin, China) overnight. Then the adherent cells were discarded and the floating cells were retained to culture using the same medium to obtain BMMs.

Construction of Genetically Engineered BMSCs: To develop RANK and CXCR4 overexpressed murine BMSCs, the lentivirus-mediated transfection was performed twice. Briefly, the coding sequences (CDS) of *Rank* (also known as *Tnfrsf11a*) and *Cxcr4* gene were obtained from NCBI and the corresponding amino acid sequences were confirmed with the help of cloud.genepioneer.com (Genepioneer Biotechnologies Co. Ltd, Nanjing, China). Firstly, the RANK-positive BMSCs were sorted using fluorescence-activated cell sorting (FACS) and subcloned when the transfection of lentivirus carrying of *Rank* gene was finished. Then these RANK-positive BMSCs were conducted another lentivirus-mediated transfection of *Cxcr4* gene. After culturing for 72 h, the transfected cells were then sorted using FACS. The CXCR4 and RANK double-positive cells were obtained and subcloned for the next study. To confirm the CXCR4 and RANK on the engineered cells, pristine or engineered BMSCs were cultured in glass bottom culture dishes designed for confocal laser scanning microscopy (CLSM) overnight. Then these BMSCs were rinsed using PBS for three times, fixed with 4% paraformaldehyde (PFA) for 10 min and permeabilized using 0.2% Triton X-100 for 10 min. After these treatments, the cells were incubated with primary antibodies of CXCR4 (R380981, ZENBIO, Chengdu, China) and RANK (also known as TNFRSF11A, A13382, ABclonal Technology) overnight. Then stained with corresponding FITC or Cy3 conjugated secondary antibodies at 4 °C for 40 min and 4′,6-diamidino-2-phenylindole (DAPI, Solarbio, Beijing, China) at 20 °C for 15 min. Finally, the fluorescence distribution and intensity were observed using CLSM.

Preparation of Engineered BMSC Membrane Coated PTH 1–34 Containing Nanogel PNG@mR&C: The nanogel was prepared as the method of previous study.[15a,31] Briefly, 0.10 mg PTH 1–34 (1.0×10^{-6} M) (KKL MED, USA) was added into 20 mL 0.1% (w/v) chitosan (Sangon Biotech, Shanghai, China) solution prepared in 1% cold acetic acid under constant stirring. Then 1.0% sodium tripolyphosphate (TPP) (Sigma Aldrich, St. Louis, MO, USA) was added dropwise into this mixture until a nanosuspension was formed. Thereafter the suspension was centrifuged at 1.0×10^5 g for 10 min using Heraeus Multifuge X1R (Thermo Fisher Scientific, Waltham, MA, USA). Then the pellet was resuspended using deionized water. The resuspended suspension was added dropwise into 10 mL PEI-DMMA (Xi'an Ruixi Biotech Co. Ltd, Xi'an, China) (0.1 mgmL) solution and stirred for 8 h at room temperature. Then the mixture was centrifuged at 1.0×10^3 g for 8 min to get rid of the large powder. The supernatant was centrifuged again at 1.0×10^4 g for 15 min to acquire the nanogel. Next, the nanogel was resuspended re-dispersed and stored at the concentration of 5 mg mL^{-1} in PBS. The zeta potential and particle size of the nanogel were detected using DLS (Brookhaven Instruments, Zeta Plus, New York, NY, USA).

The engineered BMSC membrane was prepared as reported previously.[15a] In brief, engineered BMSCs (1×10^7 cells) were treated with 1 mL reagent A of cell membrane protein extraction kit (Beyotime

Figure 6. PNG@mR&C re-established the osteoblast/osteoclast balance. A) Representative images of calcein double-labeling assays, scale bar = 100 µm. B) Quantitation of MAR ($n = 3$). C) Representative images of OCN immunofluorescent staining, OCN (green), and 4′,6-diamidino-2-phenylindole (DAPI) (blue), scale bar = 100 µm. D) Quantitation of OCN fluorescence ($n = 5$). E) Representative photographs of tartrate-resistant acid phosphatase (TRAP) staining, scale bar = 50 µm. F) Quantitation of the numbers of osteoclast (N. OCs) stained by TRAP staining ($n = 5$). G) Quantitation of receptor activator of nuclear factor-κB ligand (RANKL) concentration in the serum ($n = 5$). H–L) Quantitation of the serum concentrations of bone metabolism biochemical indicators including β-CTX, TRAP5b, BAP, OCN, and P1NP ($n = 5$). M) Relative mRNA levels of osteogenic differentiation-related genes in the femur tissues. All the values were normalized to the means of Normal group ($n = 5$). N) Relative mRNA levels of osteoclast-related genes in the femur tissues. All the values were normalized to the means of phosphate buffer saline (PBS) group ($n = 5$). O) Schematic illustration about the therapeutic effects of different drug administrations. (NS, no significant difference; $^{*}p < 0.05$; $^{**}p < 0.01$; $^{***}p < 0.001$; $^{\#}p < 0.0001$).

Biotechnology, Shanghai, China). The mixture was stored at 4 °C for 12 min and freeze–thawed repeatedly for three times. Then the mixture was centrifuged at 5.0×10^2 g for 5 min and the supernatant was centrifuged at 1.0×10^4 g for 15 min to obtain the membrane. The total protein concentration of prepared membrane was measured via a bicinchoninic acid (BCA) protein assay kit (KTD3001, Abbkine Scientific, Wuhan, China). The obtained membrane was resuspended and kept at 5 mg mL^{-1} in PBS.

For the preparation of PNG@mR&C, the cell membrane was mixed with nanogel suspension, and sonicated at 4 °C for 5 min. Then the mixture was successively extruded 15 times through polycarbonate (PC) membranes of 400- and 200- nm pores using a mini extruder (Avanti Polar Lipids, Birmingham, Alabama). The PNG@mR&C was acquired after centrifugation at 1.0×10^4 g for 15 min and re-dispersion in PBS. The zeta potential and particle size of PNG@mR&C were measured using DLS and the morphology was observed using TEM (JEM-1200EX, JEOL Ltd., Tokyo, Japan).

Protein Markers and Protein Retention Detection: The cell membrane of different genetic manipulation was extracted the total protein treated using a protein extraction kit (Beyotime). Western blot assay was used to analyze the expression of RANK and CXCR4 according to the standard protocols. Primary antibodies used in this part were RANK (ATA36616, AtaGenix Laboratories Co., Ltd., Wuhan, China) and CXCR4 (A1303, ABclonal Technology). CD90 (BS6905, Bioworld Technology, Nanjing, China) served as the control of membrane protein of BMSCs. SDS-PAGE was conducted to determine the protein contents retention of PNG@mR&C after extrusion. The SDS-PAGE colorful gel rapid preparation kit (EC0023, Shandong Sparkjade Biotechnology Co., Ltd.) was used to prepare the gel. The mR&C, PNG and PNG@mR&C were added into SDS buffer and the protein concentrations were detected with a BCA kit (Abbkine Scientific). The samples were heated at 90 °C for 3 min and 15 μg of each sample was loaded into the gel. The samples were electrophoresed at 120 V for 2 h and the gel was conducted with Commassie blue staining for 4 h and then washed for 8 h.

Transmittance Detection of PNG@mR&C Solution: To detect the transmittance of PNG@mR&C solution at various pH value, absorbance of different samples at 420 nm was determined using spectrophotometer (Thermo Fisher Scientific). Transmittance = $(1 - A_{sample}) / (1 - A_{water}) \times A_{sample}$ and A_{water} were the absorbance of solution samples and H_2O, respectively.

Cytotoxicity Assays In Vitro: Mouse BMSCs and BMMs were used to access the cytotoxicity of NG@mR&C and PNG@mR&C with a CCK-8 kit (C0005, TargetMol, Boston, MA, USA). Different cells were incubated with NG@mR&C or PNG@mR&C at different concentrations for 24 h, then the cell viabilities were detected according to the protocols.

RANKL Scavenging Assay In Vitro: The RANKL scavenging assay was conducted as previous method.[12a] Briefly, the RANKL (200 pg mL^{-1}) protein (novoprotein, Suzhou, China) was mixed with the pristine BMSC membrane vesicles (mPri), RANK-overexpressed BMSC membrane vesicles (mR), RANK and CXCR4-overexpressed BMSC membrane vesicles (mR&C), PNG or PNG@mR&C NPs at 0.25 mg membrane protein per mL or 1 mg PNG mL^{-1}. After incubation at 37 °C for 2 h and centrifuged at 1.5×10^4 g for 8 min. The concentration of RANKL in the supernatant was detected with an Enzyme-linked Immunosorbent Assay (ELISA) kit (BDEL-0306, Biodragon, Suzhou, China). To further demonstrate the RANKL scavenging function of RANK on the membrane, RANK antibodies (0.05 mg mL^{-1}) were pre-incubated with the vesicles or NPs. Then the RANK-occupied vesicles or NPs were mixed with RANKL protein, and followed by the same procedure as above.

Anti-Osteoclastogenesis Assay In Vitro: Mouse BMMs were cultured on 6-well plates (801004, NEST Biotechnology, Wuxi, China) in DMEM containing 12% FBS (UR50100, Umibio Co., Ltd., Shanghai, China), M-CSF (30 ng mL^{-1}), and RANKL (50 ng mL^{-1}) at a density of 2.5×10^5 cells (counted by automatic cell counter, Countstar BioTech, Shanghai, China) per well for 24 h. Then PBS, NG@mR&C, PTH1-34 and PNG@mR&C (100 μg NG mL^{-1}) were supplemented into the medium of these cells, respectively. The whole culture process with incubation included 24 and 120 h. After incubation for 24 h, the expressive levels of mRNA were quantified using quantitative reverse-transcription polymerase chain reaction (qRT-PCR). In addition, cells of each well were isolated from the plates and the concentrations of phosphorylated (p-) p38 (p-p38), p-JNK, and p-ERK were quantified with ELISA kits (Coibo Biotech Ltd., Shanghai, China). After incubation for 120 h, the cells were fixed with 4% PFA for 15 min, then washed three times using PBS and stained with the TRAP staining dye liquor (Sigma Aldrich). And F-actin ring staining was also conducted to display the osteoclastogenesis. The cells were fixed in PFA and washed as above, then followed incubated with Alexa Fluor 594 phalloidin (Life-iLab, Shanghai, China) for 0.5 h and DAPI Fluoromount-G (36308ES, Yeasen Biotechnology Co., Ltd., Shanghai, China) for 10 min. Finally, the stained cells were observed and photographed using a fluorescence microscope (Olympus IX71, Tokyo, Japan).

Pre-Osteoblasts and Osteoclasts Coculture: To mimic this microenvironment, pre-osteoblasts and osteoclasts coculture experiments were conducted using a transwell plate (NEST Biotechnology). The previously formed osteoclasts were reseeded on the upper chamber, and the pre-osteoblast MC3T3-E1 cells at 2.5×10^4 cells per well were cultured in the lower chamber for osteogenic differentiation induction. The bottom of lower chamber was precoated by poly-D-lysine (EN-CELL-010-2, EnoGene, Nanjing, China). After 24 h, the commercial growth medium for MC3T3-E1 (CM-0378, Procell) was removed, and MC3T3-E1 osteogenic differentiation medium (Oricell) containing PNG@mR&C (1 μg mL^{-1}) was supplemented for osteogenic induction. In the next 14 days, the medium was changed every 72 h. At Days 3 and 7, the ALP activity detection was performed with an ALP activity assay kit (BC2145, Solarbio) in accordance with the manufacturer's protocols, and the ALP staining assay was conducted using an ALP staining kit (Puhebio, Wuxi, China). At Days 7 and 14, ARS staining was performed using an ARS staining kit (Beyotime). The formation of mineralization nodules was observed with microscope. To further quantify the staining degree, 10% acetic acid was used to treat the samples overnight. Then the mixture was centrifuged, and the supernatant was treated using 10% ammonium hydroxide. Finally, 0.1 mL of each treated sample was transferred into 96-well plates and detected with a microplate reader. The absorbance at 405 nm was recorded and represented the magnitude of staining.

Immunofluorescence Staining: For detecting the expression of osteogenesis-related protein markers, MC3T3-E1 cells from different groups at Days 3, 7, and 14 of the osteogenic induction process were rinsed using PBS, then fixed with 4% PFA for 10 min, permeabilized using 0.2% Triton X-100 for 10 min. After these treatments, the cells were incubated with 1.0% BSA solution containing phalloidin-FITC (40735ES75, Yeasen Biotechnology) for 35 min and then washed using PBS. Whereafter, the primary antibodies [OSX, GB111900, Servicebio; OCN, A6205, ABclonal Technology, Wuhan, China)] diluted in antibody diluent (WB100D, New Cell & Molecular Biotech, Suzhou, China) were used to incubate the cells overnight. The primary antibodies-labeled cells were then incubated with the Cy3-conjugated goat anti-rabbit IgG (H+L) antibody (K1209, APExBIO, Houston, USA) and DAPI. The fluorescence distribution and intensity were observed using CLSM.

Biodistribution of PNG@mR&C In Vivo: To investigate the biodistribution of PNG@mR&C, the NPs were labeled with lipophilic fluorescent dye DiR (KGMP0026, KeyGEN BioTECH, Nanjing, China). These NPs were intravenously injected through the tail (1.0×10^{10} NPs dispersed in 50 μL PBS). After 4 h, the major organs were harvested from the euthanised mice and conducted for biophotonic imaging using Bruker Xtreme (Bruker Corp., Billerica, MA, USA). Bruker MI SE software was used to analyze the fluorescence intensity.

Animal Care: C57BL/6J mice (female, 12 weeks) were purchased from the Experimental Animal Centre of Huazhong University of Science and Technology (HUST), Wuhan, China. All the animal studies were approved by the Animal Experimentation Ethics Committee of HUST. The mice devoted to this study were kept in specific pathogen-free (SPF) environment and enjoyed all the animal welfares. They were arranged for four to a cage, a 12-h-light/dark cycle, with access to food and water ad libitum and a dynamic constant temperature of 25 ± 1 °C.

OVX Mice Model and Drug Administration: Mice were divided into five groups (six mice per group) randomly: Normal, PBS, NG@mR&C,

PTH 1–34 and PNG@mR&C. Except Normal group, the other groups were all conducted with bilateral OVX, while the mice of Normal group were removed some adipose around their ovaries. Intelligent anaesthesia apparatus (ZS-MV, Beijing Zhongshi Dichuang Technology Development Co., Ltd.) for small animals were used for anaesthesia in this study. In the next 8 weeks, NG@mR&C or PNG@mR&C were intravenously injected at 50 μg NG in 50 μL PBS every 3 days. To compare the therapeutic effects, the PTH 1–34 administration was accordance with the dose of common usage at 80 μg kg^{-1} d^{-1}.[32] Mice of Normal and PBS group received equivalent PBS injection served as the normal and negative control.

Blood Biochemistry and Blood Routine Examination: To determine the cytokine concentrations in serum, mouse blood samples from the ophthalmic venous plexus were obtained after anaesthesia. The venous blood was collected into the tube containing heparin and centrifuged at 1.0×10^3 g for 30 min to obtain the serum. The automated Rayto Chemray-240 chemistry analyzer (Rayto Life and Analytical Sciences Co., Ltd., Shenzhen, China) was used to conduct the blood biochemistry detection including Scr, BUN, TBil, ALT, and AST. The serum concentrations of biochemical bone markers were detected with ELISA kits according to the protocols, including P1NP, TRAP5b, BAP (P1NP, MU30602; TRAP5b, MU30923; BAP, MU30270; Bio-Swamp, Wuhan, China), β-CTX (ED-22443, AMOY LUNCHANGSHUO BIOTECH, Co., Ltd., Xiamen, China) and OCN (OCN ELISA kit, Shanghai Hengyuan Biological Technology Co., Ltd., Shanghai, China). The serum estradiol concentration was detected using Estradiol ELISA Kit (CZU02-96, Chengzhikewei Biotechnology Co., Ltd, Beijing, China). The serum RANKL and OPG concentrations were detected using RANKL ELISA Kit (Biodragon) and OPG ELISA Kit (Xinyu Biology, Shanghai, China). For blood routine examination, the whole blood was collected into the K2-ethylene diamine tetraacetic acid (EDTA) tube. The automated Mindray BC 5000 hematology analyzer (Mindray Ltd., Shenzhen, China) was used to count the blood cells numbers and analyze the parameters.

qRT-PCR: The qRT-PCR assays were performed as the protocols in the previous study.[21b] Briefly, the corresponding cells were harvested from the culture plates and treated with TsingZol Total RNA Extraction Reagent (TSP401, Tsingke Biological Technology, Beijing, China). The corresponding tissues were harvested and preserved in RNAsafety™ tissue preservation solution (01901-100, Shanghai Biotechnology Corporation) and treated with TsingZol reagent to obtain the total RNA. Then mRNA samples were reverse transcribed into complementary DNA (cDNA) with a cDNA synthesis kit (Takara, Shiga, Japan), The qRT-PCR reactions were performed with a SYBR Prime Script kit (Takara) in the BioRad CFX96 system (BioRad, California, USA). The primer serials used in this study were listed in the Table S2 (Supporting Information).

OCN Immunofluorescence Staining of Bone Tissues: The femur samples of mice were collected and fixed in 4% PFA for 1 day and then suffered 3-week decalcification using 10% EDTA. The decalcified samples were conducted 24-h dehydration using 20% sucrose solution containing 2% polyvinylpyrrolidone (PVP) at 4 °C. The dehydrated samples were then embedded with embedding medium (20% sucrose, 8% gelatine and 2% PVP) and immersed into liquid nitrogen for 30 s. Subsequently, the frozen samples in embedding medium were sliced into 10-μm sections using a freezing microtome (Leica CM3050 S). Primary antibodies of OCN (ABclonal Technology) were used to incubate with sectioned samples overnight, and the corresponding fluorescein-conjugated secondary antibodies were used to label the primary antibodies. DAPI was used to stain the cell nucleus. Finally, the sections were observed under CLSM.

H&E and TRAP Staining of Bone Tissues: The tibia samples of mice were collected and fixed in 4% PFA for 1 day and then suffered 3-week decalcification using 10% EDTA. After embedding in paraffin and slicing into 10-μm sections, the samples were conducted TRAP staining using TRAP dye liquor. The TRAP positive areas were selected and calculated with ImageJ software (NIH, Bethesda, MD, USA).

Calcein-Labeling Assays: The calciophilic fluorescence dye was used to locate the mineralization site of bone tissues. 2% sodium bicarbonate (Aladdin, Shanghai, China) solution containing 25 mg kg^{-1} calcein was administrated intraperitoneally at one week and 2 days before sacrifice. The undecalcified femur samples of mice were collected and fixed in 4% PFA for 1 day, dehydrated in 20% sucrose and embedded in methyl methacrylate. The proximal metaphysis of femurs was cut coronally into 5-mm section and observed under fluorescence microscope.

Micro-CT: The dissected femur samples were fixed with 4% PFA for 24 h, then scanned using micro-CT system Skyscan 1276 (Bruker) according to the manufacture's instruction. The region of interest (ROI) was selected from the 0.15 mm proximal to the growth plate and extended distantly for 0.4 mm. The three-dimensional images were reconstructed via CT-Vox software. The histomorphometry parameters including BMD, Tb. BV/TV, Tb. N, and Tb. Sp were analyzed via CT-An software.

Statistical Analysis: Numerical data in this study were presented as the mean ± SD. All the statistical analyses were conducted via GraphPad Prism 8.0. The statistical comparison between three or more groups was performed with one-way ANOVA, and the comparison between two groups was performed with Student's t-test. Statistical significance was appointed as NS, no statistical significance, *P < 0.05, $^{**}p < 0.01$, $^{***}p < 0.001$, and $^{\#}p < 0.0001$.

Supporting Information

Supporting Information is available from the Wiley Online Library or from the author.

Acknowledgements

Y.C., B.L., and Z.L. contributed equally to this work. The authors thank Huazhong University of Science and Technology Analytical and Testing Center Medical Sub-Center for providing the equipment of micro-CT. This research was funded by the National Natural Science Foundation of China (Grant Nos.: 81874026 and 82070911).

Conflict of Interest

The authors declare no conflict of interest.

Data Availability Statement

The data that support the findings of this study are available from the corresponding author upon reasonable request.

Keywords

biomimetic nanogels, bone-targeting, postmenopausal osteoporosis, PTH 1–34, RANKL neutralization

Received: April 26, 2023
Revised: August 22, 2023
Published online:

[1] *Am J. Med.* **1993**, *94*, 646.
[2] I. R. Reid, *Nat. Rev. Endocrinol.* **2020**, *16*, 333.
[3] J. E. Compston, M. R. McClung, W. D. Leslie, *Lancet* **2019**, *393*, 364.
[4] a) V. Fischer, M. Haffner-Luntzer, *Semin. Cell Dev. Biol.* **2022**, *123*, 14; b) C. H. Cheng, L. R. Chen, K. H. Chen, *Int. J. Mol. Sci.* **2022**, *23*, 1376.
[5] W. J. Boyle, W. S. Simonet, D. L. Lacey, *Nature* **2003**, *423*, 337.
[6] a) S. Gavali, M. K. Gupta, B. Daswani, M. R. Wani, R. Sirdeshmukh, M. I. Khatkhatay, *Biochim. Biophys. Acta, Mol. Cell Res.* **2019**, *1866*, 1498; b) Y. Matsumoto, F. Otsuka, M. Takano-Narazaki, T. Katsuyama, E. Nakamura, N. Tsukamoto, K. Inagaki, K. E. Sada, H. Makino, *Steroids* **2013**, *78*, 513.

[7] A. B. Hodsman, D. C. Bauer, D. W. Dempster, L. Dian, D. A. Hanley, S. T. Harris, D. L. Kendler, M. R. McClung, P. D. Miller, W. P. Olszynski, E. Orwoll, C. K. Yuen, *Endocr. Rev.* **2005**, *26*, 688.
[8] B. C. Silva, A. G. Costa, N. E. Cusano, S. Kousteni, J. P. Bilezikian, *J. Endocrinol. Invest.* **2011**, *34*, 801.
[9] D. L. Lacey, W. J. Boyle, W. S. Simonet, P. J. Kostenuik, W. C. Dougall, J. K. Sullivan, J. San Martin, R. Dansey, *Nat. Rev. Drug Discovery* **2012**, *11*, 401.
[10] a) R. H. Fang, A. V. Kroll, W. Gao, L. Zhang, *Adv. Mater.* **2018**, *30*, 1706759; b) G. F. Luo, W. H. Chen, X. Zeng, X. Z. Zhang, *Chem. Soc. Rev.* **2021**, *50*, 945; c) R. H. Fang, W. Gao, L. Zhang, *Nat. Rev. Clin. Oncol.* **2022**, *20*, 33; d) J. M. Spanjers, B. Stadler, *Adv. Biosyst.* **2020**, *4*, 2000174; e) Y. Chen, M. Zhu, B. Huang, Y. Jiang, J. Su, *Biomater Adv* **2023**, *144*, 213232.
[11] a) Y. Qu, B. Chu, X. Wei, Y. Chen, Y. Yang, D. Hu, J. Huang, F. Wang, M. Chen, Y. Zheng, Z. Qian, *Adv. Mater.* **2022**, *34*,2107883; b) J. Xie, Q. Shen, K. Huang, T. Zheng, L. Cheng, Z. Zhang, Y. Yu, G. Liao, X. Wang, C. Li, *ACS Nano* **2019**, *13*, 5268; c) L. Feng, C. Dou, Y. Xia, B. Li, M. Zhao, P. Yu, Y. Zheng, A. M. El-Toni, N. F. Atta, A. Galal, Y. Cheng, X. Cai, Y. Wang, F. Zhang, *ACS Nano* **2021**, *15*, 2263; d) J. Xiong, M. Wu, J. Chen, Y. Liu, Y. Chen, G. Fan, Y. Liu, J. Cheng, Z. Wang, S. Wang, Y. Liu, W. Zhang, *ACS Nano* **2021**, *15*, 19756.
[12] a) Y. Zhou, Y. Deng, Z. Liu, M. Yin, M. Hou, Z. Zhao, X. Zhou, L. Yin, *Sci. Adv.* **2021**, *7*, eabl6432; b) L. Rao, S. Xia, W. Xu, R. Tian, G. Yu, C. Gu, P. Pan, Q. F. Meng, X. Cai, D. Qu, L. Lu, Y. Xie, S. Jiang, X. Chen, *Proc. Natl. Acad. Sci. U. S. A.* **2020**, *117*, 27141; c) H. Wang, H. Liu, J. Li, C. Liu, H. Chen, J. Li, C. Sun, T. Guo, Z. Pang, B. Zhang, Y. Hu, *Bioact. Mater.* **2023**, *21*, 531.
[13] a) L. Rao, R. Tian, X. Chen, *ACS Nano* **2020**, *14*, 2569; b) Z. Li, Z. Wang, P. C. Dinh, D. Zhu, K. D. Popowski, H. Lutz, S. Hu, M. G. Lewis, A. Cook, H. Andersen, J. Greenhouse, L. Pessaint, L. J. Lobo, K. Cheng, *Nat. Nanotechnol.* **2021**, *16*, 942.
[14] M. Conceicao, L. Forcina, O. P. B. Wiklander, D. Gupta, J. Z. Nordin, B. Vrellaku, G. McClorey, I. Mager, A. Görgens, P. Lundin, A. Musaro, M. J. A. Wood, S. E. Andaloussi, T. C. Roberts, *Biomaterials* **2021**, *266*, 120435.
[15] a) L. Shang, X. Jiang, T. Yang, H. Xu, Q. Xie, M. Hu, C. Yang, L. Kong, Z. Zhang, *Acta Pharm. Sin. B* **2022**, *12*, 2550; b) Y. Zhang, K. Cai, C. Li, Q. Guo, Q. Chen, X. He, L. Liu, Y. Zhang, Y. Lu, X. Chen, T. Sun, Y. Huang, J. Cheng, C. Jiang, *Nano Lett.* **2018**, *18*, 1908.
[16] a) L. Fu, W. Zhang, X. Zhou, J. Fu, C. He, *Bioact. Mater.* **2022**, *17*, 221; b) P. Lavrador, V. M. Gaspar, J. F. Mano, *J. Controlled Release* **2018**, *273*, 51.
[17] X. Lin, Q. Wang, C. Gu, M. Li, K. Chen, P. Chen, Z. Tang, X. Liu, H. Pan, Z. Liu, R. Tang, S. Fan, *J. Am. Chem. Soc.* **2020**, *142*, 17543.
[18] T. Ono, M. Hayashi, F. Sasaki, T. Nakashima, *Inflammation Regener.* **2020**, *40*, 2.
[19] J. W. Hartley, L. H. Evans, K. Y. Green, Z. Naghashfar, A. R. Macias, P. M. Zerfas, J. M. Ward, *Retrovirology* **2008**, *5*, 1.
[20] A. Dar, P. Goichberg, V. Shinder, A. Kalinkovich, O. Kollet, N. Netzer, R. Margalit, M. Zsak, A. Nagler, I. Hardan, I. Resnick, A. Rot, T. Lapidot, *Nat. Immunol.* **2005**, *6*, 1038.
[21] a) Y. Hu, X. Li, Q. Zhang, Z. Gu, Y. Luo, J. Guo, X. Wang, Y. Jing, X. Chen, J. Su, *Bioact. Mater.* **2021**, *6*, 2905; b) Y. Cui, Z. Li, Y. Guo, X. Qi, Y. Yang, X. Jia, R. Li, J. Shi, W. Gao, Z. Ren, G. Liu, Q. Ye, Z. Zhang, D. Fu, *ACS Nano* **2022**, *16*, 11076.
[22] a) A. Kortesidis, A. Zannettino, S. Isenmann, S. Shi, T. Lapidot, S. Gronthos, *Blood* **2005**, *105*, 3793; b) X. Chen, X. Zhi, J. Wang, J. Su, *Bone Res.* **2018**, *6*, 34.
[23] R. L. Jilka, *Bone* **2007**, *40*, 1434.
[24] H. Yu, J. M. Li, K. Deng, W. Zhou, C. X. Wang, Q. Wang, K. H. Li, H. Y. Zhao, S. W. Huang, *Theranostics* **2019**, *9*, 7033.
[25] L. Chen, Y. Yang, J. Bao, Z. Wang, M. Xia, A. Dai, J. Tan, L. Zhou, Y. Wu, W. Sun, *Biomed. Pharmacother.* **2020**, *126*, 110093.
[26] Y. Kim, M. D. Brodt, S. Y. Tang, M. J. Silva, *Methods Mol. Biol.* **2021**, *2230*, 169.
[27] R. D. Bloebaum, B. M. Willie, B. S. Mitchell, A. A. Hofmann, *J. Biomed. Mater. Res., Part A* **2007**, *81*, 505.
[28] a) Y. L. Ma, R. L. Cain, D. L. Halladay, X. Yang, Q. Zeng, R. R. Miles, S. Chandrasekhar, T. J. Martin, J. E. Onyia, *Endocrinology* **2001**, *142*, 4047; b) E. G. Estell, C. J. Rosen, *Nat. Rev. Endocrinol.* **2021**, *17*, 31.
[29] L. Song, *Adv. Clin. Chem.* **2017**, *82*, 1.
[30] C. J. Li, Y. Xiao, Y. C. Sun, W. Z. He, L. Liu, M. Huang, C. He, M. Huang, K. X. Chen, J. Hou, X. Feng, T. Su, Q. Guo, Y. Huang, H. Peng, M. Yang, G. H. Liu, X. H. Luo, *Cell Metab.* **2021**, *33*, 1957.
[31] D. Narayanan, A. Anitha, R. Jayakumar, S. V. Nair, K. P. Chennazhi, *J. Biomed. Nanotechnol.* **2012**, *8*, 98.
[32] a) N. Tokuyama, J. Hirose, Y. Omata, T. Yasui, N. Izawa, T. Matsumoto, H. Masuda, T. Ohmiya, H. Yasuda, T. Saito, Y. Kadono, S. Tanaka, *Bone Rep* **2015**, *2*, 1; b) T. Yamamoto, T. Hasegawa, M. Sasaki, H. Hongo, K. Tsuboi, T. Shimizu, M. Ota, M. Haraguchi, M. Takahata, K. Oda, P. H. Luiz de Freitas, A. Takakura, R. Takao-Kawabata, Y. Isogai, N. Amizuka, *Endocrinology* **2016**, *157*, 2604; c) C. L. Henaff, F. Ricarte, B. Finnie, Z. He, J. Johnson, J. Warshaw, V. Kolupaeva, N. C. Partridge, *J. Bone Miner. Res.* **2020**, *35*, 714.